A&A manuscript no.
(will be inserted by hand later)
⋆ ⋆⋆
Your thesaurus codes are:
03 11.03.4; 11.09.1; 11.09.3; 12.04.1; 13.25.2; 12.03.3

ASTRONOMY
AND
ASTROPHYSICS
1.2.2008

X-ray analysis of Abell 2634 and its central galaxy 3C465

Sabine Schindler@1,2,* & M. Almudena Prieto@1,**

@1 Max-Planck-Institut für extraterrestrische Physik, Giessenbachstraße, D-85748 Garching, Germany @2 Max-Planck-Institut für Astrophysik, Karl-Schwarzschild-Straße 1, D-85748 Garching, Germany

[the date of receipt and acceptance should be inserted later]

Abstract. An analysis of a ROSAT/PSPC observation of the galaxy cluster A2634 is presented. It has a luminosity of $7.9 \pm 0.1 \times 10^{43}$erg/s in the ROSAT band (0.1-2.4 keV). The temperature profile decreases from about 3 keV in the outer parts to 1.2 keV in the centre. Within a radius of 1.5 Mpc the gas mass of the cluster is $0.51 \times 10^{14} \mathcal{M}_{\odot}$ and the total mass amounts to $4.1^{+2.6}_{-1.8} \times 10^{14} \mathcal{M}_{\odot}$. The X-ray morphology shows two peculiar features – a strongly peaked emission in the centre and an excess emission in the south-west. The central emission probably originates from a weak cooling flow, the SW emission is possibly associated with higher density regions in pressure equilibrium with the intra-cluster medium. This region of excess emission is somewhat embraced by the wide-angle radio tails associated with 3C465 suggesting that the overpressure of the relativistic particles has displaced the thermal gas.

Key words: Galaxies: clusters: individual: A2634 - Galaxies: individual: 3C465 - inter-galactic medium - dark matter - X-rays: galaxies - Cosmology: observations

1. Introduction

A2634 is a nearby Abell cluster at z=0.0293 (Scodeggio et al. 1995) of richness class I. The dominant central object is the radio-galaxy 3C465 (or NGC 7720), a prototype wide-angle tailed (WAT) source of moderate radio power, $F(178\text{MHz}) = 6.4 \times 10^{37}$ Jy (Laing et al. 1983) and narrow optical emission lines.

A2634 is projected onto a complex region in the sky dominated by large-scale structure associated with the Pisces-Perseus supercluster. A detailed description of the 12 degrees field around A2634 can be found in Scodeggio et al. (1995). Briefly, the region includes several clusters and groups; yet, none of them are found gravitationally bound to A2634.

The spatial distribution of the cluster members, their kinematics and dynamics were studied extensively in Scodeggio et al's work on the basis of optical and radio data. The authors find the properties of the early-type population component being in agreement with those expected from a relaxed system, whereas the opposite is found for the spiral population, whose multimodal velocity distribution and lack of concentration towards the cluster core suggest their recent arrival to the system. However, the lack of significant clumpiness in the galaxy distribution argues against a merger event to have occurred in the plane of the sky. A remaining possible option would be the possibility that loose groups of spirals were falling onto the cluster along the line of sight.

Pinkney et al. (1993) provided a different view of A2634. The authors reported on a peculiar radial velocity of more than 200 km/s to be associated with the central galaxy. They found substructure in the outer parts of the cluster and concluded that A2634 is an unrelaxed cluster with an ongoing merger. Burns et al. (1993) explained the radio and X-ray appearance of A2634 as being in a post-merger state.

In this paper, we further explore the dynamical state of A2634 on the basis of a detailed analysis of the ROSAT/PSPC data of the cluster. The spatial distribution of the PSPC X-ray light and the associated dynamics are compared with the spatial distribution of the cluster galaxies and their kinematics as derived from the optical study by Scodeggio et al. (1995). Furthermore, the PSPC spectral information is used to determine the temperature of the intra-cluster gas and cluster mass. Finally, possible origins for the bending tailed radio structure associated with the central galaxy and its relationship with the hot cluster medium are discussed.

$H_0 = 50$ km/s/Mpc is used throughout. 1 arcsecond is about 850 pc at the distance of A2634.

⋆ e-mail: sas@mpa-garching.mpg.de
⋆⋆ e-mail: alm@mpe-garching.mpg.de

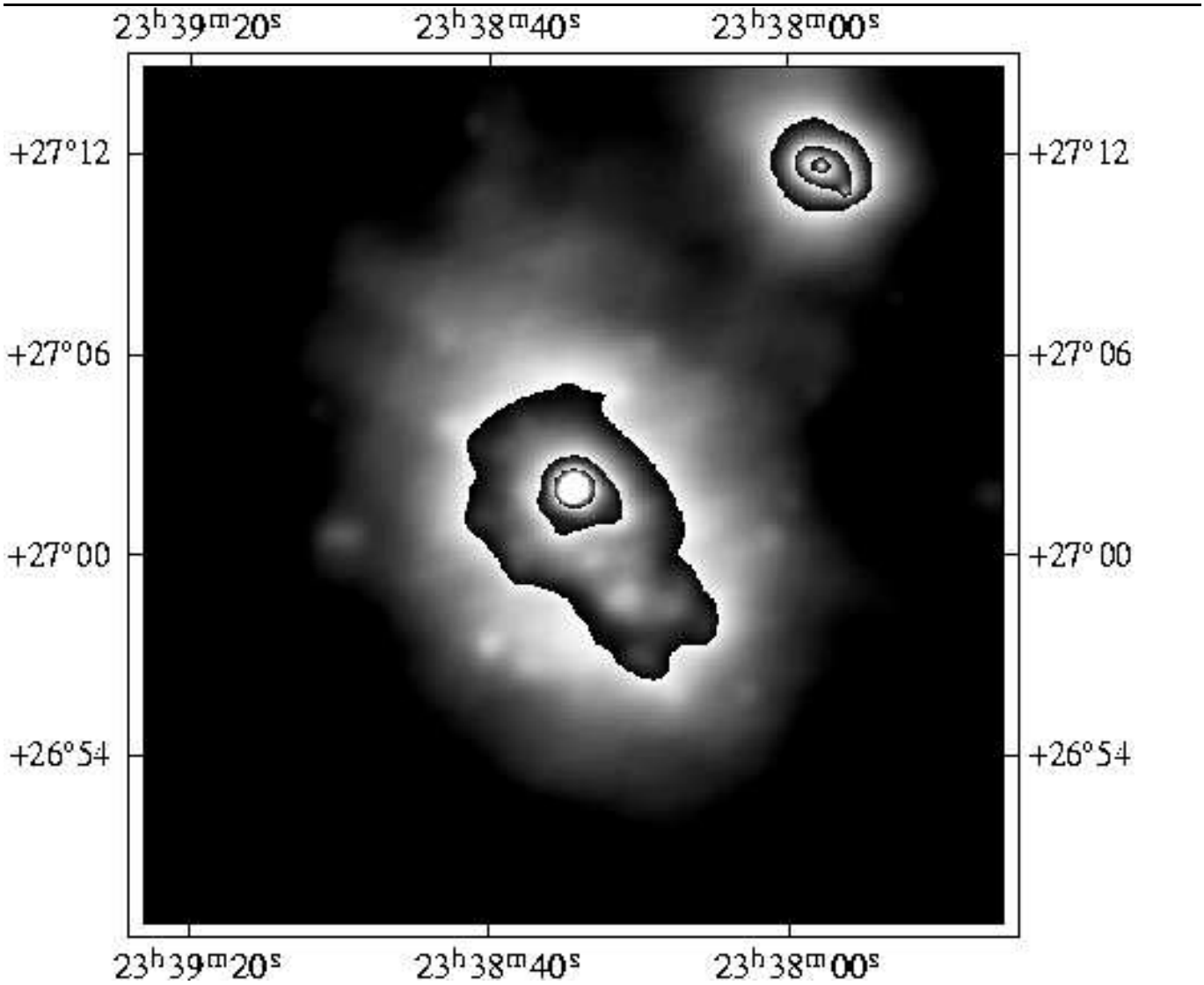

Fig. 1. ROSAT/PSPC image of the cluster A2634 in the ROSAT hard energy band (0.5-2.0 keV). It is smoothed with a Gaussian filter of σ varying from 1.8 arcseconds to 1.4 arcminutes. The X-ray image is dominated by the emission centred on 3C465 and shows substructure in the south-west. The emission in the north-west of A2634 is associated with the cluster CL-37.

2. Data

A2634 was observed in a pointed observation with the ROSAT/PSPC on June 20$^{\rm th}$ to 22$^{\rm th}$, 1991. The total effective exposure time was 9100 sec. The central galaxy of the cluster, 3C465, was placed at the centre of the PSPC field-of-view. To flat-field the image, corresponding energy-weighted exposure maps are derived and subsequently combined according to the energy distribution of the source. The data are then divided by these maps. Finally, a Gaussian filter with σ varying from 1.8 arcseconds to 1.4 arcminutes is applied to the data. The resulting accumulated image in the 0.5-2 keV band is shown in Fig. 1.

The most prominent emission feature in the X-ray image is at the centre and coincides with the position of 3C465 and its companion galaxy, the latter being located $\sim$ 12 arcseconds to the north from 3C465 (Fig. 2). HST/WFPC2 images of the field taken in the R band reveal no signs of interaction between the two objects, both showing well defined elliptical isophotes. The two galaxies both show prominent rings of dust (Fig 2.). VLBI observations (Venturi et al. 1995) reveal the central conspicuous morphology of the core region of 3C465.

The ROSAT/HRI image of the cluster (Sakelliou & Merrifield 1997) also shows one single point source at the centre of the cluster. We thus expect the peak of the central X-ray emission to be coincident with the 3C465 radio core position.

The second bright source in Fig. 1 (upper-right corner of the figure) is associated with the background cluster

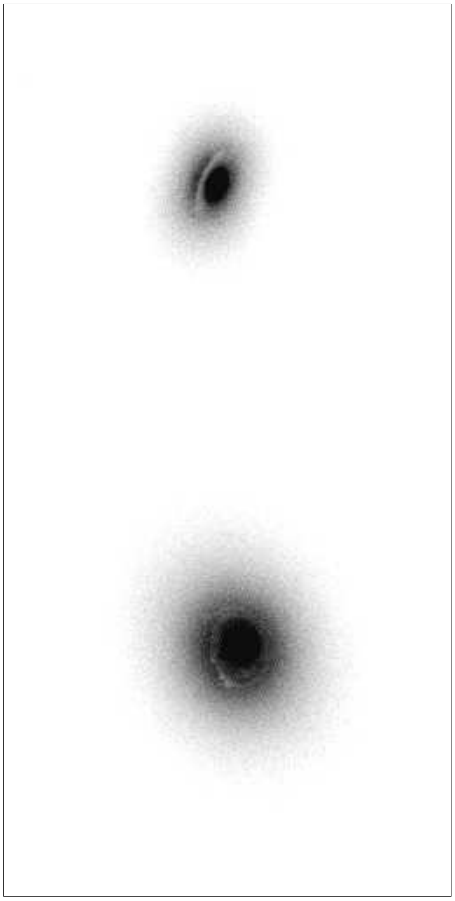

Fig. 2. HST/WFPC2 image of 3C465 (bottom) and its companion galaxy observed with the F702W filter. Both galaxies show prominent dust lanes. The distance between the centres of the two galaxies is 12 arcseconds.

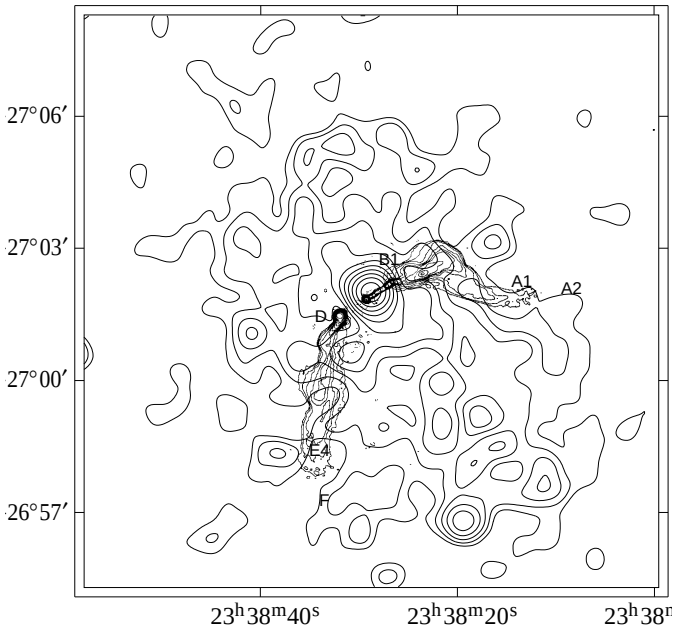

Fig. 3. 5 GHz VLA map (Venturi et al. 1995) superposed on contours of a PSPC image smoothed with a Gaussian filter of $\sigma = 15$ arcsec. The spacing of the X-ray contours is logarithmic with 10 contours per order of magnitude. The highest contour line corresponds to a countrate of 9.2×10^{-4} counts/s/arcmin^2.

CL-37 (z∼0.123, Scodeggio et al. 1995), which is projected $\sim$ 13 arcminutes from the centre of A2634.

The diffuse X-ray emission associated with A2634 shows clearly an elongation in NE - SW direction. This asymmetry is particularly pronounced within the $\sim$ 6 arcminutes inner radius. Excess emission above the diffuse average level is apparent in the south-west region of the cluster, where a somewhat elongated and patchy structure is clearly seen (Fig. 1). This excess emission was already seen in previous EINSTEIN IPC maps of the cluster (Eilek et al. 1984) though with much less spatial detail due to the poorer spatial resolution of the IPC (FWHM $\sim$ 1.5 arcmin).

Fig. 3 presents a logarithmic contour image of the central field shown in Fig. 1, also from the same energy band, 0.5-2 keV. The 5 GHz VLA map by Venturi et al. (1995) is overlaid (see also Burns et al. 1993). The inferior resolution of the PSPC hampers any detailed comparison between the radio and X-ray data; yet, one can readily see that the overall distribution of the extended radio emission avoids somewhat that of the X-ray emission. Although projection effects can affect the comparison, in the apparent distribution the kiloparsec-scale jet associated with the central galaxy 3C465 extends almost perpendicular to the main direction of the X-ray emission. Both radio tails give the impression to open their way through the hot medium by bending and propagating along regions of lower X-ray surface brightness. In particular, the X-ray surface brightness is low in the direction of the tails around a radius of about 1 arcminute (see also Fig. 6).

3. Spatial analysis

The X-ray emission in A2634 can grossly be resolved in three main components: a symmetric region of diffuse emission extending into the Mpc range, an inner region of enhanced emission and peculiar morphology distributed in south-westerly direction extending up to about 6 arcminutes ($\sim$ 300 kpc) from the centre, and finally, an unresolved peaked emission at the centre. The corresponding ROSAT/HRI image of the cluster (cf. Fig. 1 in Sakelliou & Merrifield 1997) confirms the peaked central emission and the elongation of the overall X-ray structure in the NE-SW direction.

To quantify the asymmetry of the diffuse X-ray emission, ellipses of different isophote levels are fitted to the PSPC image (cf. Bender & Möllenhoff 1987). Relatively high eccentricities of 0.3 - 0.5 between the surface brightness levels 1.6×10^{-3} and 4.3×10^{-3} cts/s/arcmin^2 (Fig. 4) are found, which are caused by the excess emission to

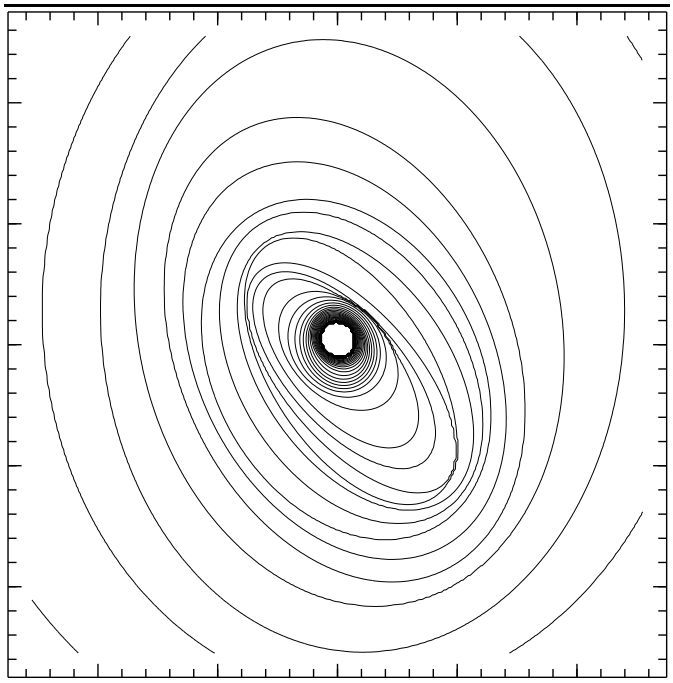

Fig. 4. Ellipse fits to different isophote levels. The original image is exposure corrected and smoothed with a Gaussian filter with $\sigma = 25$ arcsec. We find large eccentricities of 0.3 - 0.5 in NE-SW direction at surface brightness levels of 1.6×10^{-3} to 4.3×10^{-3} cts/s/arcmin^2. The size of the image is 21.3×21.3 arcmin^2.

the south-west of the maximum. The ellipses within this interval have position angles between 20° and 50° (north is 0, counterclockwise). These angles agree well with the outer optical isophotes of 3C465 (de Juan et al. 1994) although the X-ray isophotes reach up to much larger radii (the major axes in this interval are between 2.3 and 9.6 arcminutes). The agreement between the optical and X-ray rotation angles was previously found from the EINSTEIN IPC X-ray image (Pinkney et al. 1993).

As the outer region of the cluster shows small eccentricities, the cluster surface brightness profile is derived assuming spherical symmetry (Fig. 5). As centre, the maximum of the X-ray emission at $\alpha = 23^h38^m29^s$, $\delta = +27°02'00''$ (J2000) is used. It differs by about 8 arcseconds from the radio core coordinates (Venturi et al. 1995), which is consistent with the expected ROSAT pointing errors. Only photons in the ROSAT hard band (0.5-2.0 keV) are considered. Nine sources around the cluster which are probably fore- or background sources are excluded from the profile extraction. Two of these nine sources are seen in Fig.1: CL-37 and the point-like source on the central-left side of the image at $\alpha = 23^h39^m00^s$, $\delta = +27°00'40''$ (J2000).

The resulting light profile is fitted with a β-model (Cavaliere & Fusco-Femiano 1976; Jones & Forman 1984):

$$\Sigma(r) = \Sigma_0 \left(1 + \left(\frac{r}{r_c}\right)^2\right)^{-3\beta+1/2}, \quad (1)$$

where Σ_0 is the central surface brightness, r_c is the core radius, and β is the slope parameter. The central bins ($r < 30$ arcseconds) are excluded for the fit because they are obviously dominated by the emission of the central source. A fit of the region between 30 arcseconds up to 5 arcminutes from the centre yields $\Sigma_0 = 3.4 \times 10^{-3}$ counts/s/arcmin^2, $r_c = 9.8^{+1.3}_{-1.1}$arcmin (490^{+70}_{-50}kpc), and $\beta = 0.79^{+0.10}_{-0.07}$ (1σ errors). The results for the fit parameters do not change significantly when varying the radial binning.

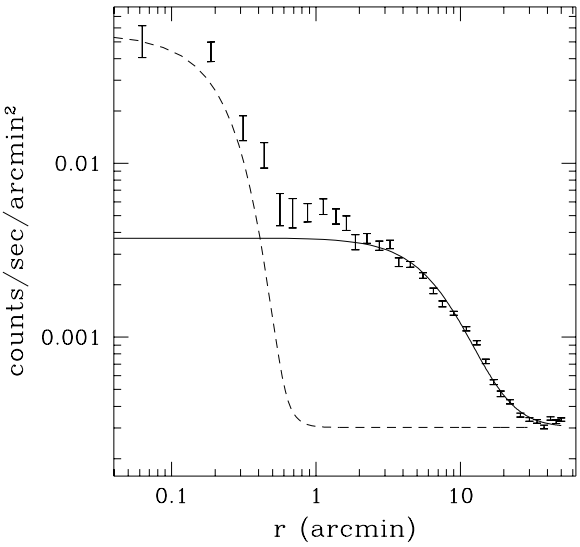

Fig. 5. Radial profile of the hard band (0.5-2.0 keV) emission of A2634. The solid line is a fit with a β-model. The four innermost bins are ignored by the fit because they are dominated by the central source. Owing to the elongation of the cluster we find a relatively large core radius of $r_c = 490$kpc. For comparison also the point spread function of the ROSAT/PSPC normalized to the central bin is plotted (dashed line).

Taking into account that the cluster is more extended in south-westerly direction, independent fits are applied to the south-west and north-east profiles, respectively. In the north-east (-45° to 135°), very similar values to the overall profile values are found: $\Sigma_0 = 3.1 \times 10^{-3}$ counts/s/arcmin^2, $r_c = 9.7$arcmin, and $\beta = 0.75$, whereas the fit to the south-west profile gives a larger core radius as well as a larger β, which reflects the observed elongation in this direction. The resulting fit parameters in this

case are: $\Sigma_0 = 3.6 \times 10^{-3}$ counts/s/arcmin^2, $r_c = 11.0$ arcmin, $\beta = 0.91$.

To make the excess emission visible, a synthetic, spherically symmetric image with the parameters of the overall β-fit is constructed. When subtracting the synthetic image from the PSPC image, two separated regions of enhanced emission are readily seen (Fig. 6). Besides the unresolved emission in the centre, enhanced emission along the NE-SW direction is revealed, the excess being more prominent towards the south-west region of the cluster. Note that the most prominent regions of enhanced emission are already apparent in the original PSPC image (Fig. 1 and 3). The significance of this excess emission is determined using the method developed by Neumann & Böhringer (1997). A significance of 10σ is derived for the central emission, the two maxima in the south-west part having significances of 5σ and 4σ, respectively. Besides, the derived model subtracts fairly well the X-ray distribution in other parts of the cluster, indicating that the diffuse intracluster emission is compatible with spherical symmetry.

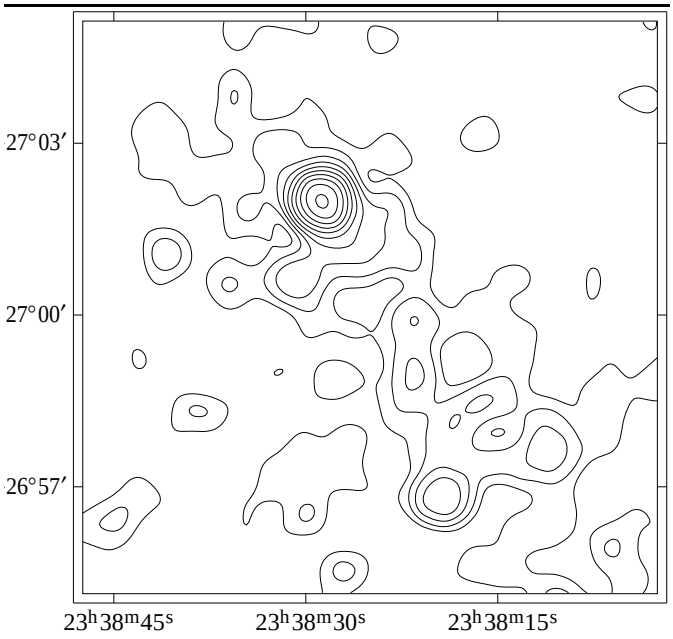

Fig. 6. Residual image after subtracting a spherically symmetric image constructed with a β profile with $\Sigma_0 = 3.4 \times 10^{-3}$ counts/s/arcmin^2, $r_c = 9.8$arcmin, and $\beta = 0.79$ centred on the X-ray maximum from an image smoothed with Gaussian filter of $\sigma = 15$arcsec. The contours represent the significance of emission above the β profile in units of σ. The excess emission in the centre has a significance of 10σ. The two maxima in the south-west have significances of 5σ and 4σ, respectively.

4. Spectral analysis

The brightness and proximity of A2634 permits the collection of a sufficient number of photons for a spectral analysis to be performed. The primary objective is to determine whether a temperature variation does exist across the cluster. Individual spectra are accumulated from different regions in the cluster. The size and the number of regions are a compromise between adequate spatial resolution and the inclusion of a sufficient number of counts for a reliable fit to be performed.

Individual spectra are extracted from three consecutive concentric rings: an outer one, comprising the region between 5.5 and 9.5 arcmin, an intermediate one between 3 and 5.5 arcmin, and an inner one, between 1.5 and 3 arcmin. The spectrum of the central region is derived from a region of 1 arcminute radius. In addition, an average temperature of the cluster is derived from a fit to the whole diffuse emission region excluding a central region of 1.5 arcminutes radius.

Each spectrum is fitted with a Raymond & Smith model (1977). The limited number of photons within each of the rings together with the relatively soft energy range of the PSPC prevents a simultaneous fitting of all parameters: metallicity, hydrogen column density, temperature and the flux normalization factor. Thus, the metallicity is fixed to a typical cluster value of $m = 0.35$ (Arnaud et al. 1992; Yamashita 1994; Tsuru et al. 1996). Table 1 summarizes the main fit results.

Table 1. PSPC spectral analysis: parameters are derived from a single Raymond-Smith model with fixed metallicity $m = 0.35$. Errors are 1 sigma correlated multi-parameters uncertainties. Fit^a corresponds to a power-law fit, the parameter marked is the power-law index. SW is the south-west sector defined by angles from 180 to 245 degrees (north over east) and radii as indicated.

radius [arcmin] $1' \sim 50$ kpc	total counts	temperature [keV]	$n_{\rm H}$ [10^{21}cm^{-2}]	χ^2/dof
1.5 - 11.0	5700	$3.5^{+1.2}_{-0.7}$	0.6 ± 0.1	1.0/90
5.5 - 9.5	2500	$3.5^{+2.0}_{-1.0}$	$0.4^{+0.2}_{-0.0}$	0.7/49
3.0 - 5.5	1700	$3.5^{+2.5}_{-1.0}$	0.6 ± 0.1	1.3/45
1.5 - 3.0	700	$4.0^{+5.0}_{-1.0}$	0.6 ± 0.1	1.1/32
centre - 1.0	270	$1.2^{+0.2}_{-0.1}$	0.9 ± 0.4	0.6/31
centre - 1.0^a	270	$-5.4^{+1.7a}_{-2.2}$	$6.5^{+3.5}_{-3.0}$	0.7/29
SW: 1.3 - 7.0	670	$1.6^{+0.8}_{-0.2}$	$0.8^{+0.3}_{-0.2}$	1.2/31
SW: 1.0 - 1.3	210	$1.4^{+1.4}_{-0.2}$	$0.4^{+0.2}_{-0.0}$	1.0/30

All the performed fits have in common, that the derived values for $n_{\rm H}$ are within the errors in excellent agreement with the Galactic value in the direction of A2634: $n_{\rm H} = 0.52 \times 10^{21}$ cm^{-2} (Dickey & Lockman 1990). Well constrained temperatures are obtained in the centre of the cluster, $1.2^{+0.2}_{-0.1}$ keV (Fig. 7) and in the outermost ring, $3.5^{+2.0}_{-1.0}$ keV (Fig. 8). The fit to the overall diffuse emission

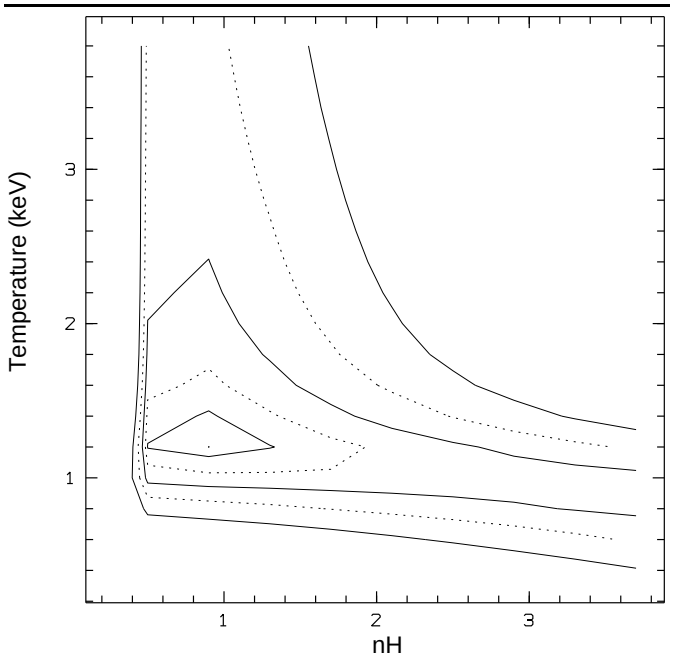

Fig. 7. Confidence contours for the fit parameters temperature and hydrogen column density ($n_{\rm H}$ in units of 10^{21} cm^{-2}) for a Raymond-Smith-model fit to the central 1 arcminute region. The contours span 1 to 5 σ.

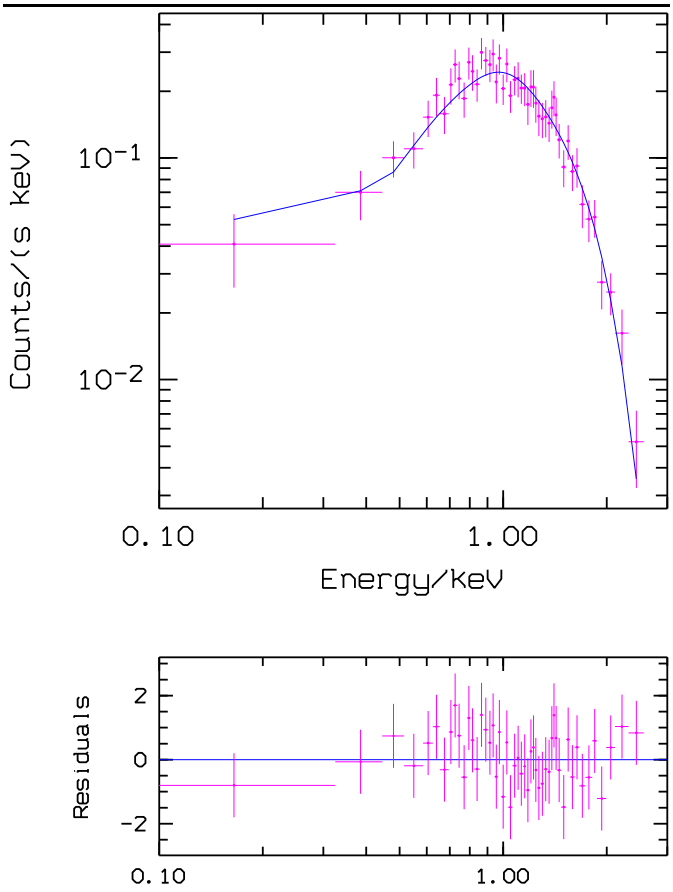

Fig. 8. PSPC spectrum of the cluster region between 3 and 5.5 arcminutes from the centre. The solid line is a fit with a Raymond-Smith model with fixed metallicity $m = 0.35$ and fit parameters as in Table 1. The bottom panel shows the fit residuals in sigma units.

region is also well constrained (Fig. 9), giving a cluster average temperature of $3.5^{+1.2}_{-0.7}$ keV. The spectra from the two inner rings are statistically poorer. For these two rings, fixing $n_{\rm H}$ to the Galactic value sligthly modifies the χ^2 of the fit, but hardly changes the temperature.

The light profile shown in Fig. 5 indicates that the emission in the inner 1 arcminute of the cluster is unresolved. It is dominated by strongly peaked emission at the centre compatible with the ROSAT/PSPC point-spread-function, the contribution of the extended gas emission being no larger than 1%. Since there is a radio galaxy in the centre of the cluster, one might expect most of the central emission to be of non-thermal nature. For testing this hypothesis we fit the spectrum from the central 1 arcminute region separately with a power-law model and a thermal model. We find that the power-law model leads to extreme spectral indices and to an $n_{\rm H}$ being more than an order of magnitude higher than the Galactic value for a statistically acceptable fit (Fig. 10, Table 1). Therefore we consider this model to be unrealistic. On the other hand a Raymond-Smith model provides a good representation of the central PSPC spectrum, leading to a $n_{\rm H}$ in fair agreement with the corresponding Galactic value (Fig. 7, Table 1). Thus the *dominant* emission appears to be of thermal origin.

In addition, separate fits are attempted over several regions in the south-west region of the cluster. A first fit is applied to the region between 1.3 and 7 arcminutes from the centre comprising angles between 180° − 245° (north over east). The central emission and the two blobs of bright emission seen close to the centre are excluded. The total number of counts, ∼ 670 counts, slightly exceeds that from other equivalent quadrants in the cluster, which have of the order of 400 counts on average. A temperature of $1.6^{+0.8}_{-0.2}$ keV is found, which virtually fits in between the slighter lower temperature in the central region and the higher one in the outer regions of the cluster.

A second separate fit is attempted for the region comprising the two blobs of brighter emission seen immediately close to the centre of the cluster in the south-westerly direction. The accumulated spectrum includes the region between 1 and 1.3 arcminutes from the centre and is defined by the same angles as above. Although the accumulated number of counts is relatively low, ∼ 200, both temperature and $n_{\rm H}$ are constrained in the fit. The temperature of ∼ 1.4 keV is just following the general trend of decreasing temperatures towards the centre of the cluster.

Summarizing, a consistent decreasing temperature gradient towards the centre of the cluster is measured in A2634. This is supported by the two fairly well constrained

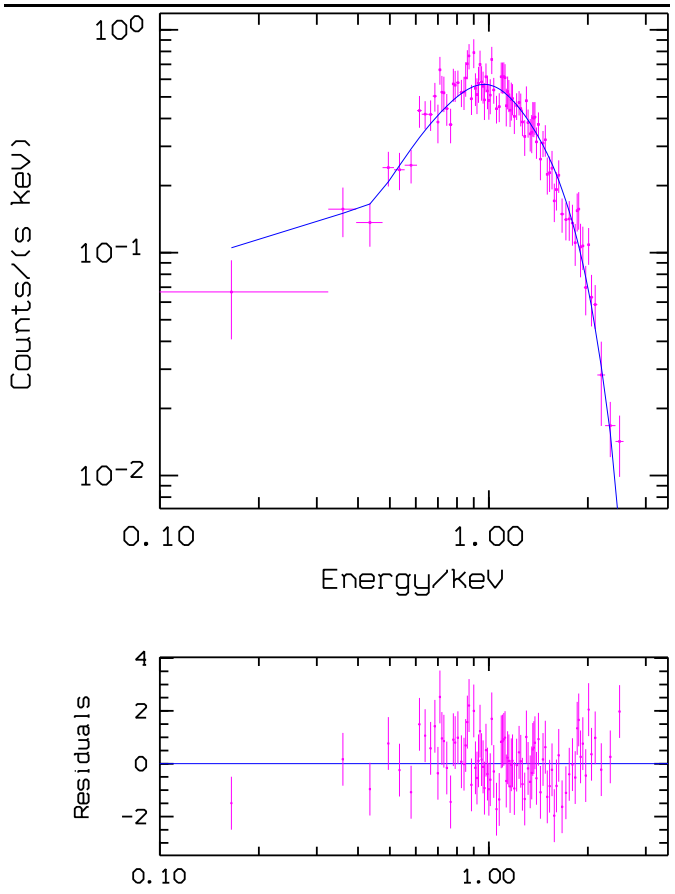

Fig. 9. PSPC spectrum of the cluster region between 1.5 and 11 arcminutes from the centre. The solid line is a fit with a Raymond-Smith model with fixed metallicity $m = 0.35$ and fit parameters as in Table 1. The bottom panel shows the fit residuals in sigma units.

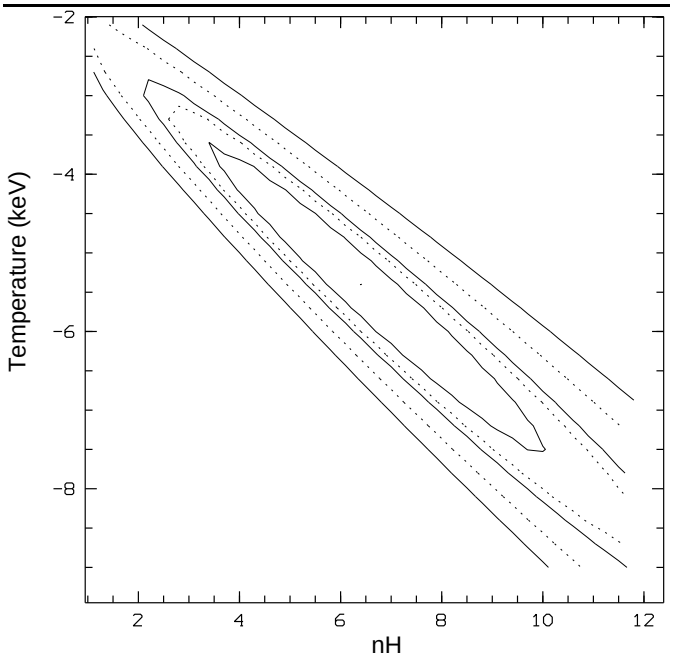

Fig. 10. Confidence contours for the fit parameters power-law index and hydrogen column density ($n_{\rm H}$ in units of 10^{21} cm^{-2}) derived from a power-law fit to the central 1 arcminute region of A2634. The contours span 1 to 5 σ.

temperatures of about 3 and 1.2 keV derived for the outermost and for the inner 1 arcminute region of the cluster, respectively. The south-west region of excess emission shows marginal evidence for lower temperatures below 3 keV. A recent analysis of ASCA data of A2634 (Fukazawa, private communication) is also consistent with a decreasing temperature towards the centre and with the south-west region being of lower temperature.

5. Luminosity

The cluster emission can be traced out to a radius of about 30 arcminutes (1.5 Mpc). Within this radius a count rate of 1.1 counts/s (only source counts; excluding the emission of CL-37) is obtained. Assuming an average cluster temperature of $3.5^{+1.2}_{-0.7}$ keV (as derived in Sect. 4, see Table 1), a Galactic hydrogen column density of 0.52×10^{21}cm^{-2} and an average cluster metallicity of 0.35 solar, that count rate corresponds to a luminosity of $7.9 \pm 0.1 \times 10^{43}$ erg/s in the ROSAT band (0.1 - 2.4 keV) and a bolometric luminosity of $1.4 \pm 0.3 \times 10^{44}$ erg/s. The errors only refer to the uncertainty in the temperature.

The luminosity in the central 1 arcminute inner region is 2.2×10^{42}erg/s (0.1-2.4 keV). This has been derived using the parameter values listed in Table 1. The contribution from the extended gas emission is inferred, following the spatial analysis of Sect. 3 (Fig. 5), to be less than 1%.

6. Mass determination

The fit parameters of the β model: $\Sigma_0 = 3.4 \times 10^{-3}$ counts/s/arcmin^2, $r_c = 9.8$arcmin and $\beta = 0.79$, are used to make a deprojection of the 2D image to get the three dimensional density distribution. In doing so, it is assumed that the clumpiness of the gas and local temperature variations do not affect the mass estimate grossly. The corresponding gas mass profile is shown in Fig. 11. Within a radius of 1.5 Mpc, the gas mass amounts to $5.1\times10^{13}\mathcal{M}_\odot$.

With the additional assumption of hydrostatic equilibrium, the integrated *total* mass is calculated from the equation

$$M(r) = \frac{-kr}{\mu m_p G} T \left(\frac{d\ln\rho}{d\ln r} + \frac{d\ln T}{d\ln r} \right), \qquad (2)$$

where ρ and T are the density and the temperature of the intra-cluster gas, and r, k, μ, m_p, and G are the radius, the Boltzmann constant, the molecular weight, the proton mass, and the gravitational constant, respectively. The assumption of hydrostatic equilibrium is well justified even

when assuming that the excess emission in the south-west region corresponds to an infalling subcluster. This excess luminosity of this region is less than 2% of the total luminosity of the cluster. Converting this luminosity fraction to a mass fraction we find that the subcluster represents only 10% of the total cluster mass which is too small to introduce significant deviations from an equilibrium configuration.

In the central 1 arcminute, a mass determination is hardly possible, because the most important factor in Eq. 2 – the density gradient – is dominated by the point spread function of the PSPC. Therefore, this region of the cluster is excluded when deriving the total mass. The rest of the cluster is considered to be isothermal with an average temperature of $3.5^{+1.2}_{-0.7}$ keV (Table 1). The profile of the integrated mass is shown in Fig. 11. As we cannot determine the temperature beyond 550 kpc, we assume that the temperature in the outer parts is the same as between 75 and 550 kpc. If using the β fit parameters that are derived from the north-east part of the cluster, i.e. the region less affected by substructure (Sect. 3), the corresponding mass profile is essentially the same.

At a radius of 1.5 Mpc the derived total mass is $4.1^{+2.6}_{-1.8} \times 10^{14} \mathcal{M}_{\odot}$. The errors only reflect the uncertainty in the cluster temperature (including possible temperature gradients within the error range). The systematic errors are probably much smaller (Schindler 1996a; Evrard et al. 1996). For comparative purposes, the total mass derived from the X-ray observation is in agreement with the viral mass, $5.2 \times 10^{14} \mathcal{M}_{\odot}$, derived by Scodeggio et al. (1995) for the same cluster radius.

The gas mass fraction at 1.5 Mpc radius is found to be 12^{+10}_{-5}% and increases very slightly with radius.

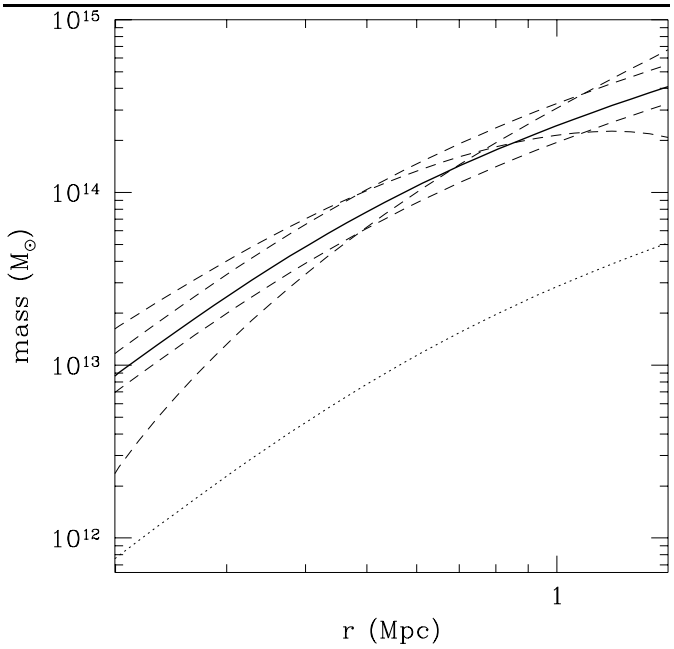

Fig. 11. Profile of the integrated total mass (full line) between 0.2 and 1.5 Mpc with errors coming from the uncertainty in the overall temperature and possible temperature gradients within the error range (dashed lines). The dotted line shows the profile of the integrated gas mass.

7. Central emission

As shown in Sect. 4, the centrally peaked emission in A2634 is well described by a single, *thermal* spectral component. Though non-thermal emission due to the central radio source would also be expected, the thermal component appears, however, to be the dominant component of the emission.

The integrated 0.1-2.4 keV luminosity from the inner 1 arcmin, $L_X = 2.2 \times 10^{42}$erg s^{-1}, places A2634 within the lower power range of X-ray luminosities measured in the central region of clusters dominated by FRI radio sources (Prieto 1996). In general, the X-ray luminosities in those cases span a range of $10^{42} - 10^{44}$erg s^{-1}, and mostly reflect the cluster emission.

The central $n_{\rm H}$ derived from the spectral fit falls within the average range of values found in our Galaxy. Thus it is unlikely that high absorption is the cause for the AGN source to be undetected. An HST/WFPC2 image of 3C465 in the filter F702W reveals clearly a thick ring of dust surrounding the galaxy bulge (Fig. 2). The central source may be partially obscured by this material but not completely as the plane of the ring is almost face-on with respect to the line of sight. All facts together suggest that most probably the AGN activity in 3C465 is presently very weak.

3C465 is a cD galaxy. This property together with the measured temperature drop in the centre of the cluster are suggestive of a cooling flow scenario. As it is shown below, parameters derived from the present X-ray data are compatible with a weak cooling flow.

The central electron density of the cluster is determined using a *composite* β model. The β model used in Sect. 3 accounts well for the emission distribution beyond a radius of 2 arcminutes from the centre (see Fig. 5); yet, if only this model would be used to derive the central density, the density would be underestimated by more than an order of magnitude. Thus, to account properly for the central emission, a second β model is fit to the residual image resulting after subtracting the β model of Sect. 3. This second β model fits the residual image up to a radius of 37 arcseconds from the centre.

An estimate of the cooling flow parameters are derived from the sum of both β models. The central electron density is found to be 0.016cm^{-3}, which yields a central cooling time of about 3×10^9 yr. This time is considerably smaller than the Hubble time, thus an equilibrium situation could have established. With the usual assumptions (i.e., a cooling time smaller than 10^{10} yr) a cooling flow

radius of about 25 arcseconds ($\sim$ 20 kpc) is derived. Using the approximation:

$$L_{\rm cool} = \frac{5}{2}\frac{\dot{M}}{\mu m}kT, \quad (3)$$

the derived mass accretion rate within that radius is about 1 $\mathcal{M}_\odot$/yr. Unfortunately, the central emission is not resolved (see Fig. 5), therefore we cannot see the true extent of the cooling flow. Thus the derived radius of 20 kpc is actually an upper limit.

8. Comparison with optical data

Evidence for cluster substructure has been found in a substantial number of EINSTEIN images (e.g. Forman & Jones 1982; Mohr et al. 1993) and presently, better resolved, in ROSAT images (e.g. A2256, Briel et al. 1991; Virgo, Böhringer et al. 1994; A3528, Schindler 1996b; A3627, Böhringer et al. 1996; CL0939+4713, Schindler & Wambsganss 1996; CL0016+16, Neumann & Böhringer 1997). Regions of excess X-ray emission in clusters are usually interpreted as the signature of a subcluster or galaxy group being in the process of merging with the main cluster. As such, the south-west X-ray enhancement in A2634 may also be indicative of subclustering.

Potential optical counterparts to the X-ray excess region are sought on the basis of the optical study of the cluster members by Scodeggio et al. (1995). Judging from the apparent spatial distribution of the cluster galaxies, no obvious correspondence with either individual members or groups of them is found. Indeed, Scodeggio et al. remarked on the lack of significant clumpiness in both the kinematic and the spatial distribution of the galaxy members. They found, however, a clear morphological segregation between the early- and the late-type galaxy population: E and S0 are spread all over the cluster; S and Irr are almost absent in the central region of the cluster. Since the region of X-ray excess arises in the inner ($\sim$ 6 arcmin) region of the cluster, it may only be related, if anything, to the early-type population members. Focusing on the central 20 arcminutes of the cluster (cf. Fig. 14 in Scodeggio et al. 1995), a certain level of alignment of the cluster galaxies in the direction close to the major axis of 3C465 is apparent. This direction is roughly coinciding with that marked by the south-west excess region. While the combined effect could just reflect an asymmetric central potential, we note that, first, the galaxies concentration is more accentuated in the north-east side of the cluster rather than in south-west where most of X-ray excess arises; second, the overall extended emission appears compatible with spherical symmetry (see Sect.3).

If focusing on the kinematic of the early-type population members, their spatial and kinematic distribution of velocities (Scodeggio et al. 1995) are also found compatible with those expected from a dynamically relaxed system.

Thus, on the basis of both kinematic and morphology of the cluster galaxies, the observed X-ray excess in A2634 is unlikely to be associated with a subcluster or group falling into the cluster. As a final cross-check, the Palomar plates are examined for potential unrelated sources lying in the direction of the cluster. Both red and blue plates are examined and no association with any outstanding X-ray feature is found. Therefore, on the basis of the available optical data, the X-ray excess emission in the south-west region of A2634 appears to be unrelated with any visible mass distribution.

9. The X-ray / radio relationship

Fig. 3 compares the X-ray and radio emission in A2634. Projection effects hamper a clear determination of the relative distribution of both emissions and thus, on their possible interaction. Nevertheless, Fig. 3 clearly shows the 3C465 radio jet extending perpendicular to the direction of X-ray excess region. Also, the wide angle tails that characterize the radio structure bend along the same *projected* directions on the sky, thus, are virtually embracing the south-west X-ray excess region.

An alternative way to probe the dynamical state of the system is to verify whether the gas and plasma pressures are in equilibrium. To this end, equipartition pressures in the tails, as derived by Eilek et al. (1984), are compared with thermal pressures derived from the present ROSAT data. The latter are obtained under the assumption of spherical symmetry. The density values derived from the two added β models (Sect. 7) are adopted.

For those regions in the tails far away from the centre, E4, F, A1 and A2 (see Fig. 3; nomenclature by Riley & Branson 1973), thermal and equipartition pressures are found in balance, in agreement with what was found by Eilek et al. (1984) on the basis of EINSTEIN IPC data. However, for those regions closer to the centre, i.e., D and B1, which are roughly at the position where respective tails begin to open, thermal pressures are found a factor 2 - 5 smaller than the equipartition pressures. For the intermediate regions no temperatures are available (see Table 1); yet, when interpolating between the inner and the outermost temperature an increasing discrepancy towards the centre is found. While individual pressure values may be uncertain due to the number of involved assumptions, the tendency for an increasing pressure imbalance towards the centre of the cluster should be regarded as a more solid result, and it would imply that the system is not yet in an equilibrium configuration.

10. Discussion and Conclusions

Two particular features characterize the X-ray image of A2634: strongly peaked emission at the centre and a region of enhanced emission in the south-west area of the cluster. In addition, the system is embedded in a spherical gas region which can be traced up to ∼1.5 Mpc from the cluster centre.

Within the spatial and spectral limitations of the PSPC data, a cooling flow scenario arises as the best interpretation for the central emission in A2634. There are several arguments supporting this scenario: the thermal nature of the central spectrum, the presence of a cD galaxy and the temperature drop at the centre (the central temperature is found to be 1.2 keV while the average intracluster gas is about 3.5 keV). The temperature drop is also confirmed by ASCA (Fukazawa, private communication).

Within the cooling flow radius of 20 kpc we derive a relatively small mass accretion rate of about 1 $\mathcal{M}_\odot$/yr. The mass accretion rate falls, nevertheless, within the range of values derived from the correlation between mass accretion rates, luminosity and temperature in cooling flow clusters (Fabian et al. 1994). For comparative purposes, the prototype cooling flow in Virgo (M87) presents a cooling flow radius of 70 kpc (also for a cooling time smaller than 10^{10} yr) and a mass accretion rate of about 10 $\mathcal{M}_\odot$/yr (Stewart et al. 1984). The situation of A2634 seems closer to Fornax, where a mass accretion rate of 2 $\mathcal{M}_\odot$/yr within a radius of 40 kpc was derived (Rangarajan et al. 1995). The cooling flows in Virgo and Fornax could, however, be resolved as they are much closer than A2634.

The expected AGN contribution due to the central source 3C465 is not readily detected in the PSPC band. The 0.1-2.4 keV central spectrum appears instead dominated by a thermal component, moderately absorbed by a $n_{\rm H}$ in close agreement with the Galactic value. The fact that no excess absorption is found towards the cluster centre lead us to the conclusion that the AGN source rather than be obscured is in a quiescent period.

The presence of enhanced X-ray emission in the south-west region of the cluster motivates the search for optical counterparts that could be related to a potential subcluster or group in interaction with A2634. Previously, Pinkney et al. (1993) and Burns et al. (1993) already suggested a merging scenario for A2634. However, on of the basis of both observational and theoretical considerations we find the merging scenario unlikely. The X-ray excess region shows no correspondence with the spatial distribution of the cluster members, nor with their corresponding spatial distribution of velocities. A comparison with hydrodynamic simulations of subcluster collisions (Schindler & Müller 1993) shows that in the case of a *post-merging phase*, the intracluster gas is squeezed out by the merger to show up as hot bulges in directions perpendicular to the collision axis. However, the region of enhanced X-ray emission in A2634 shows a well defined elongated distribution which is likely defining, if anything, the direction of the potential encounter. On the other hand, in a *pre-merging phase*, the simulations predict the formation of a heated region between the two parties as soon as they get closer than about 1-2 Mpc. Such a feature is not seen in the temperature map of the cluster. Instead, the temperature measurements in the south-west region are consistent with a progressive decay towards the centre of the cluster. This temperature drop in south-westerly direction is also confirmed by ASCA data (Fukazawa, private communication).

A2634 can be classified as a poor cluster. It has a low X-ray luminosity, $1.4\pm0.3\times10^{44}$erg/s (bolometric) if compared with other clusters of similar optical richness (class I). The inferred mass, $4.1^{+2.6}_{-1.8}\times10^{14}\mathcal{M}_\odot$, is at the lower limit of the typical mass range in clusters, $5-50\times10^{14}\mathcal{M}_\odot$, as well as the gas mass fraction, about 12%, compared with typical values in clusters, 10-30% (Böhringer 1995).

On the other hand, the basic cluster parameters are consistent with each other and with the general relations found in clusters. Relative to the bolometric luminosity the average cluster temperature falls into the expected range (e.g. Edge & Stewart 1991a; David et al. 1993; White 1996). The velocity dispersion of 661 km/s (Scodeggio et al. 1995) also lies within the $\sigma - T$ relation (Edge & Stewart 1991b; Lubin & Bahcall 1993; Bird et al. 1995).

A2634 has many properties in common with the Virgo cluster: It has about the same luminosity and is only slightly more massive (Böhringer 1995). Virgo is a prototype cooling flow, and also shows X-ray substructure (Böhringer et al. 1994). The associated radio emission in M87 is, however, correlated in position with the X-ray emission (Böhringer et al. 1995), while in A2634 the radio structure opens its way along directions perpendicular to the region of enhanced X-ray emission. This anti-correlation resembles the situation in the Perseus cluster, where the X-ray emission shows minima at the positions of the radio lobes (Böhringer et al. 1993) suggesting that the pressure of the relativistic particles has displaced the thermal gas.

The radio emission associated with 3C465 shows a well defined configuration. The 3C465 radio jet is seen extending perpendicular to the direction of enhanced X-ray emission and both radio tails appear to embrace virtually the south-west X-ray excess region. Pressure equilibrium between the relativistic plasma and the intra-cluster medium is found at the outer parts of the radio tails. However, an increasing imbalance is measured towards the inner regions of the cluster, the plasma pressure being found larger than that of the gas. This overpressure is indicative that the system may not have reached an equilibrium configuration yet. No visible mass is seen associated with the south-west excess region, so it is plausible that part of the X-ray substructure seen in that region just reflects an inhomogeneous density medium, perhaps being produced

Table 2. Summary of the X-ray properties of A2634

L_X(0.1-2.4keV)	$7.9 \pm 0.1 \times 10^{43}$erg/s
L_X(bol)	$1.4 \pm 0.3 \times 10^{44}$erg/s
count rate(0.1-2.4keV)	1.1counts/s
r_c	$9.8^{+1.3}_{-1.1}$arcmin (490^{+70}_{-50}kpc)
β	$0.79^{+0.10}_{-0.07}$
$M_{gas}(r < 1.5\mathrm{Mpc})$	$0.51\times10^{14}\mathcal{M}_\odot$
$M_{tot}(r < 1.5\mathrm{Mpc})$	$4.1^{+2.6}_{-1.8} \times 10^{14}\mathcal{M}_\odot$
gas mass fraction	$12^{+10}_{-5}\%$
central cooling time	3×10^9yr
mass accretion rate of possible cooling flow	$\sim 1\mathcal{M}_\odot$/yr

by the displacement of the gas by the plasma flow. The decreasing temperature gradient measured in this region would then be consistent with the formation of cooler gas condensations in equilibrium with the surrounding intracluster gas.

Acknowledgements.

It is a pleasure to thank Hans Böhringer and Doris Neumann for helpful discussions. S.S. acknowledges financial support by the Verbundforschung.

References

Arnaud M., Rothenflug R., Boulade O., Vigroux L., Vangioni-Flam E., 1992, A&A 254, 49
Bender R., Möllenhoff C., 1987, A&A 174, 63
Bird C.M., Mushotzky R.F., Metzler C.A., 1995, ApJ 453, 40
Böhringer H., 1995, in: Proceedings of the 17^{th} Texas Symposium on Relativistic Astrophysics and Cosmology, Böhringer H., Morfill G.E., Trümper J.E. (eds.), New York Academy of Sciences, New York, p. 67
Böhringer H., Voges W., Fabian A.C., Edge A.C., Neumann D.M., 1993, MNRAS 264, L25
Böhringer H., Briel U.G., Schwarz R.A., Voges W., Hartner G., Trümper J., 1994, Nat 368, 828
Böhringer H., Nulsen P.E.J., Braun R., Fabian A.C., 1995, MNRAS 274, L67
Böhringer H., Neumann D.M., Schindler S., Kraan-Korteweg R., 1996, ApJ 467, 168
Briel U.G., Henry J.P., Schwarz R.A., Böhringer H., Ebeling H., Edge A.C., Hartner G.D., Schindler S., Trümper J., Voges W., 1991, A&A 246, L10
Burns J.O., Rhee G., Roettiger K., Owen F.N., 1993, in: ASP Conference Series, Vol. 51, Observational Cosmology, Chincarini G., Iovino A., Maccacaro T., Maccagni D. (eds.), ASP, San Francisco, p. 407
Cavaliere A., Fusco-Femiano R., 1976, A&A 49, 137
David L.P., Slyz A., Jones C., Forman W., Vrtilek S.D., Arnaud K.A., 1993, ApJ 412, 479
de Juan L., Colina L., Pérez-Fournon I., 1994, ApJS 91, 507
Dickey J.M., Lockman F.J., 1990, ARA&A 28, 215
Edge A.C., Stewart G.C., 1991a, MNRAS 252, 414
Edge A.C., Stewart G.C., 1991b, MNRAS 252, 428
Eilek J.A., Burns J. O., O'Dea C., Owen F.N., 1984, ApJ 278, 37
Evrard A.E., Metzler C.A., Navarro J.F., 1996, ApJ 469, 494
Fabian A.C., Crawford C.S., Edge A.C., Mushotzky R.F., 1994, MNRAS 267, 779
Forman W., Jones C., 1982, ARA&A 20, 547
Jones C., Forman W., 1984, AJ 276, 38
Laing R.A, Riley J.M., Longair M.S., 1983, MNRAS 204, 151
Lubin M.L., Bahcall N.A., 1993, ApJ 415, L17
Mohr J.J., Fabricant D.G., Geller M.J., 1993, ApJ 413,492
Neumann D.M., Böhringer H., 1997, MNRAS 289, 123
Pinkney J., Rhee G., Burns J.O., Hill J.M., Oegerle W., Batuski D., Hintzen P, 1993, ApJ 416, 36
Prieto M.A., 1996, NRAS 282
Rangarajan F.V.N., Fabian A.C., Forman W.R., Jones C., 1995, MNRAS 272, 665
Raymond J.C., Smith B.W., 1977, ApJS 35, 419
Riley J.M., Branson N.J.B.A., 1973, MNRAS 164, 271
Sakelliou I., Merrifield M.R., 1997, MNRAS, submitted
Schindler S., 1996a, A&A 305, 756
Schindler S., 1996b, MNRAS 280, 309
Schindler S., Müller E., 1993, A&A 272, 137
Schindler S., Wambsganss J., 1996, A&A 313, 113
Scodeggio M., Solanes J.M., Giovanelli R., Haynes M.P., 1995, ApJ 444, 41
Stewart G.C., Canizares C.R., Fabian A.C., Nulsen P.E.J., 1984, ApJ 278, 536
Tsuru T., Koyama K., Hughes J.P., Arimoto N., Kii T., Hattori M., 1996, in: UV and X-Ray Spectroscopy of Astrophysical and Laboratory Plasmas, Yamashita K., Watanabe T. (eds.), Universal Academic Press, Tokyo, p. 375
Venturi T., Castaldini C., Cotton W.D., Feretti L., Giovannini G., Lara L., Marcaide J.M., Wehrle A.E., 1995, ApJ 454, 735
White D.A., 1996, in: Röntgenstrahlung from the Universe, Zimmermann H.U., Trümper J.E., Yorke H., MPE report 263, p. 621
Yamashita K., 1994, in: Clusters of Galaxies, Durret F., Mazure A., Trân Thanh Vân J. (eds.), Edition Frontieres, Gif-sur-Yvette, p. 153

This article was processed by the author using Springer-Verlag TEX A&A macro package 1992.